

# Characterization of trace gas emissions from controlled laboratory burning of Canadian boreal forest fuels

Rowshon Afroz<sup>1</sup>, Hongru Shen<sup>2,3</sup>, Bradley H. Isenor<sup>2</sup>, Samar G. Moussa<sup>4</sup>, Amanda Hanashiro Moraes<sup>1</sup>, Shakiba Talebian<sup>1</sup>, Carolyn Liu-Kang<sup>2</sup>, Jeremy J. B. Wentzell<sup>4</sup>, Oscar Olfert<sup>5</sup>, Amy Leithead<sup>4</sup>, Ginny Marshall<sup>6</sup>, Ralf M. Staebler<sup>4</sup>, Cris Mihele<sup>4</sup>, Arthur W. H. Chan<sup>7</sup>, Jason Olfert<sup>5</sup>, John Liggio<sup>3</sup>, Jonathan Abbatt<sup>2</sup>, Ran Zhao<sup>1</sup>, and Sumi N. Wren<sup>4</sup>

<sup>1</sup>Department of Chemistry, University of Alberta, Edmonton, Alberta, Canada

<sup>2</sup>Department of Chemistry, University of Toronto, Toronto, Ontario, Canada

<sup>3</sup>School of Environmental Science and Engineering, Shanghai Jiao Tong University, Shanghai, China

<sup>4</sup>Air Quality Research Division, Environment and Climate Change Canada, Toronto, Ontario, Canada

<sup>5</sup>Department of Mechanical Engineering, University of Alberta, Edmonton, Alberta, Canada

<sup>6</sup>Natural Resources Canada, Edmonton, Alberta, Canada

<sup>7</sup>Department of Chemical Engineering and Applied Chemistry, University of Toronto, Toronto, Ontario, Canada

**Correspondence:** Sumi N. Wren (sumi.wren@ec.gc.ca)

Section S1: Structural classification of compounds quantified by Vocus PTR-MS and I-CIMS.

Section S2: I-CIMS and Vocus PTR-MS calibration.

Section S3: Biomass sample characterization.

Section S4: Characterization of emissions by biomass type.

5 Section S5: Biomass burning literature.

Section S6: Dependence of NMOC,  $\sum$  VOCs, and individual VOC emission factors (EF) on modified combustion efficiency (MCE).

Section S7: Principal component analysis (PCA).

Section S8: Reactive nitrogen emission factors

10 Section S9: Additional Canadian Forest Fire Emissions Prediction System (CFFEPS) details.

Section S10: Dependence of  $\text{NMOC}_G$  ( $\text{g kg}^{-1}$ ) on MCE.

A list of supplementary tables (Tables S1 - S5) is included here for reference, while the complete tables are provided in the accompanying supplementary Excel file.

15 Table S1: Summary of measured compounds, including molecular information, instrumentation, sensitivities, calibration methods, and uncertainties.

Table S2: Detailed information of fuel properties, combustion efficiency, duration, and phase-resolved emissions data of measured species across different biomass types.

Table S3: The mean overall and combustion-phase resolved emission ratio data of measured species across different biomass

20 types.

Table S4: Literature-reported emission factors used for comparison with the present study.

Table S5: List of literature used for comparison, including study type, biomass, source table, average MCE, and additional notes.

## 25 Section S1: Structural classification of compounds quantified by Vocus PTR-MS and I-CIMS

The double bond equivalent (DBE) is a widely used metric to represent the degree of unsaturation in a molecule, calculated using Equation (S1) (Gilman et al., 2015; Roson et al., 2024; Koch and Dittmar, 2006). Thus, this approach is used to gain insight into the structures and reactivities of compounds in complex mixtures, such as those found in biomass burning emissions.

$$\text{DBE} = C + \frac{N}{2} - \frac{H}{2} + 1 \quad (\text{S1})$$

30 where C, H, and N represent the number of carbon, hydrogen, and nitrogen atoms, respectively.

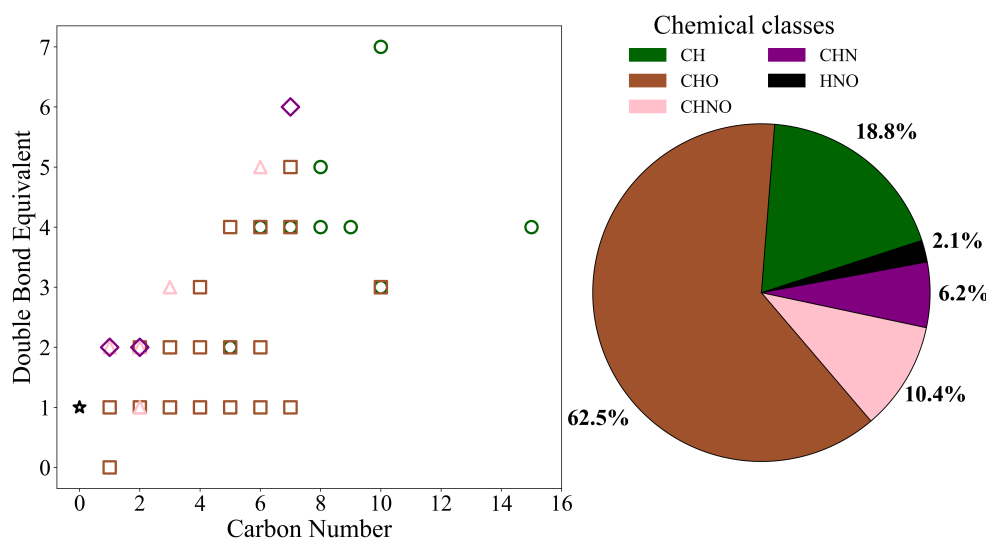


**Figure S1.** DBE versus carbon number distribution (left) and percentage contribution of each chemical class composition in the pie chart (right) of VOCs and inorganic gases measured/calibrated from the studied biomass burning samples.

Figure S1 summarizes the molecular characteristics of the 47 species quantified by Vocus PTR-MS and I-CIMS (46 VOC + HONO). The compounds were classified into five chemical groups: hydrocarbons (CH), oxygenated hydrocarbons (CHO), oxygen- and nitrogen-containing hydrocarbons (CHNO), nitrogen-containing hydrocarbons (CHN), and nitrogen–oxygen species (HNO). The pie chart shows that CHO compounds are the most abundant, accounting for 62.5 % of all measured species. They are followed by CH at 18.8 %, CHNO at 10.4 %, CHN at 6.2 %, and HNO at 2.1 %.

The left panel presents the DBE versus carbon number plot, which illustrates the structural diversity of the quantified compounds (Gilman et al., 2015; Roson et al., 2024; Koch and Dittmar, 2006). The five chemical groups span carbon numbers from C1 to C15 and DBE values from 0 to 7, representing saturated, unsaturated, aliphatic, aromatic, and oxygenated structures.

## Section S2: I-CIMS and Vocus PTR-MS calibration

### 40 I-CIMS calibration

Calibrations for the majority of the volatile organic compounds (VOC) were performed using a home-built liquid calibration unit (LCU) in which dilute aqueous solutions of known concentration were nebulized into a heated evaporation chamber with zero air sheath gas flow. The delivered mixing ratio was controlled via the liquid flow rate and dilution gas flows.

Hydrogen cyanide (HCN) was calibrated using a cylinder (1 ppm in balance of N<sub>2</sub>). The nitrous acid (HONO) standard  
45 was generated in-house by passing a humidified hydrochloric acid flow in nitrogen through a permeation oven packed with glass beads coated in a saturated aqueous sodium nitrite solution (the hydrochloric acid permeation tube and sodium nitrite permeation oven were both held at 40° C). The isocyanic acid (HNCO) standard was generated via the thermal decomposition of cyanuric acid (250° C). HONO and hydrogen cyanide were quantified as NO using a Thermo Scientific 42i chemiluminescent instrument after passing over an external molybdenum converter (heated to ~ 325° C) to convert NO<sub>y</sub> to NO. Isocyanic acid  
50 was quantified using the same method after passing the isocyanic acid flow through a heater at ~ 770° C. Standards were diluted in zero air (AADC0 generator) and humidified as necessary using a second nebulizer and heated evaporation chamber.

Humidity-dependent calibrations were performed for the majority of compounds, and sensitivities were determined as a function of the iodide-water adduct (I<sub>I·H<sub>2</sub>O</sub><sup>-</sup>)/iodide (I<sub>I</sub><sup>-</sup>) signal ratio,  $\theta$ , to yield  $S_M(\theta)$ , parameterized as linear or exponential functions of  $\theta$ .

$$55 \quad \theta = \frac{I_{I \cdot H_2O^-}}{I_{I^-}} \quad (S2)$$

For all compounds measured with the I-CIMS, normalized ion signals were converted to mixing ratios using measured sensitivities,  $S_M(\theta)$ , where  $\theta$  was derived by averaging pre-burn measurements of  $\theta$  across all burns.

$$X_M(\text{ppbv}) = \frac{X_M(\text{ncps})}{S_M(\theta)(\text{ncps ppbv}^{-1})} \quad (S3)$$

The typical value of  $\theta$  was  $\approx 0.43$ . For practical reasons, calibrations were performed under ‘dry’ conditions only (50 sccm  
60 humidified N<sub>2</sub> flow only) for some compounds. For these calibrations, the value of  $\theta$  was  $\approx 0.43$ , similar to what was observed during the burns. Mixing ratios were corrected for dilution for the EF calculations. A list of the calibrated compounds and their sensitivities is provided in SI Table S1. Uncertainties for calibrations with gas standard cylinders and the liquid calibration unit are estimated at ~ 20 %, while uncertainties for calibrations using home-assembled permeation tubes or custom sources are estimated at ~ 30 % (Hayden et al., 2022).

### 65 Vocus PTR-MS calibration:

The daily multi-point calibration cylinder contained methanol, acetonitrile, acetaldehyde, acetone, isoprene, benzene, toluene, 3-hexanone, xylene, 1,2,4-trimethylbenzene, 1,2-dichlorobenzene, 1,2,4-trichlorobenzene, D3-siloxane, and D4-siloxane. Stan-



dards were diluted in zero air generated by passing ambient air through the Pt catalyst in the Vocus calibration unit (Aerodyne Research Inc.). Sensitivities for additional VOCs (SI Table S1) were determined via calibrations performed before and/or after the campaign using additional standard cylinders and three other approaches. A home-built calibration system was used to deliver and dilute calibrants from a) aqueous solutions nebulized into a heated evaporation chamber (i.e., the home-built LCU), b) home-assembled permeation tubes, and c) vapour of pure liquid calibrant in a temperature-controlled glass diffusion tube. For the latter two approaches, the mixing ratio of the delivered calibrants was determined by passing the output through a quartz tube heater (400° C) and quantifying as CO<sub>2</sub> using a Picarro CO<sub>2</sub>-CO-CH<sub>4</sub> analyzer (G2401-m). The pre- and post-campaign sensitivities were corrected using the daily calibration sensitivities, which varied by 10-27 % on average. Uncertainties for calibrations with gas standard cylinders and the liquid calibration unit are estimated at ~ 20 %, while uncertainties for calibrations using home-assembled permeation tubes or diffusion tubes are estimated at ~ 30 % (Hayden et al., 2022; Pfannerstill et al., 2023; Coggon et al., 2024).

While multiple isomers could contribute to signal at a given  $m/z$  (i.e., the calibrated compound and other isomers), sensitivities for PTR-MS across all species and  $m/z$  generally do not vary by more than a factor of ~ 2 – 4 (Pagonis et al., 2019; Jensen et al., 2023; Link et al., 2025). During BBCan, the Vocus PTR-MS was (inadvertently) operating with so-called “Mag-Mode” activated, resulting in enhanced sensitivities across an apparent  $m/z$  window ~ 80 – 130, compared to ranges typically reported in the literature for PTR operating under similar conditions (Link et al., 2025; Jensen et al., 2023). Nonetheless, it is expected that VOCs with the same exact mass will have sensitivities that vary considerably less than a factor of 2, given the dependence of PTR sensitivity on the PTR rate coefficient ( $k_{PTR}$ ), which depends on molecular properties, including molecular weight, polarizability, and dipole moment (Sekimoto et al., 2017). Fragmentation of larger ions could also contribute to signal at a given  $m/z$  (Coggon et al., 2024), and calculated mixing ratios (and therefore EF) should be considered an upper limit.

### Section S3: Biomass sample characterization

Samples were placed in glass petri dishes, wrapped in parafilm, and stored at -20° C until ready for use. Each ‘dry’ sample was initially placed in a controlled drying room maintained at 40° C for several days to reduce its natural moisture content and simulate typical pre-ignition wildfire conditions. On the other hand, the ‘wet’ samples were thawed one week before the experiments and held at ambient temperature and humidity to allow their moisture content to equilibrate with the surrounding air. To determine the moisture content, a representative subsample from each fuel type was weighed before and after oven-drying at 95° C. This process ensured the removal of all remaining moisture. The moisture content ( $\phi$ ) was then calculated using Equation (S4), based on the difference between the wet and dry weights.

$$\phi = \left( \frac{\text{Mass of sample} - \text{Mass of oven dried sample}}{\text{Mass of oven dried sample}} \right) \times 100\% \quad (\text{S4})$$

Elemental composition (e.g., % C, N, H, S by mass) of the fuels was analyzed using a Thermo Flash 2000 Elemental Analyzer. For this analysis, aliquots of wet and dry biomass samples were homogenized to ensure representative elemental characterization. Additional details regarding biomass collection and characterization are provided in the BBCan lab campaign overview paper (Moraes et al., 7 May 2026).

## Section S4: Characterization of emissions by biomass type

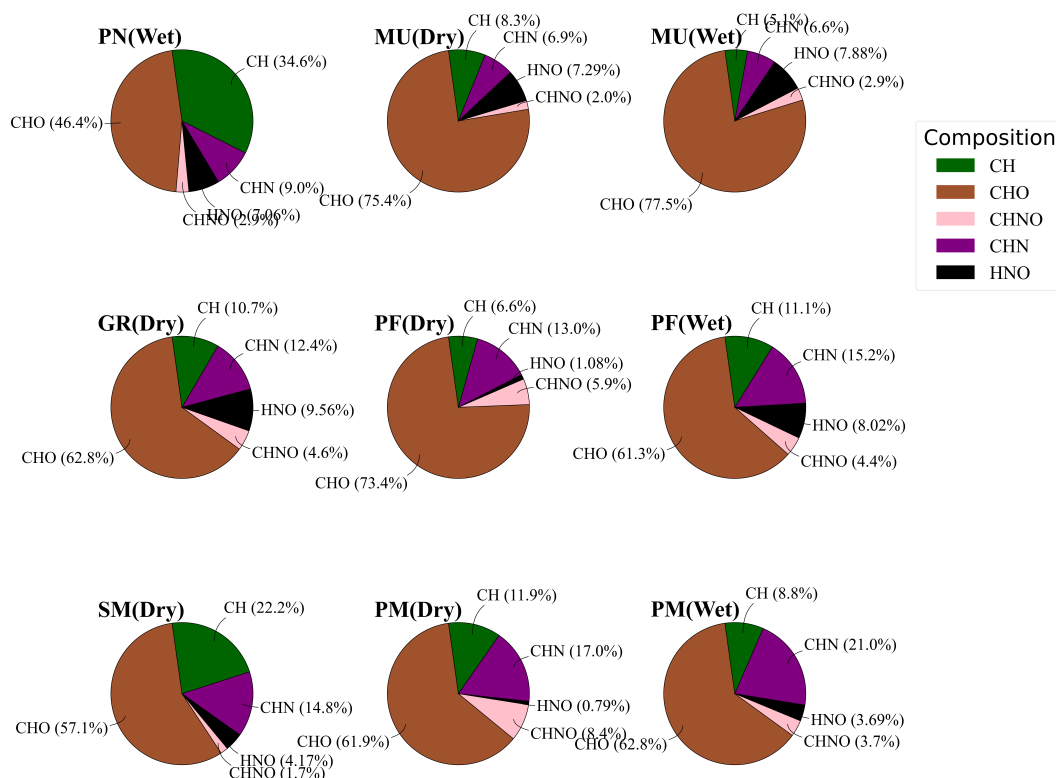


**Figure S2.** Contribution of chemical classes (CH, CHO, CHNO, CHN, HNO) to  $\sum \text{VOCs EF}$  ( $\text{g kg}^{-1}$ ) for the studied biomass fuels.

## Section S5: Biomass burning literature

Individual VOC EF for the various biomass types and moisture conditions are compared to literature studies in Fig. 2, Fig. 5, and Fig. S5. These studies are chosen to capture a range of emission conditions and fuel types relevant to boreal wildfires and the fuels targeted in this study. For molecular formulae with multiple isomers reported, the EFs are first summed (e.g., for  $\text{C}_{10}\text{H}_{16}$ , EFs for all reported monoterpenes are summed). Table S2 in the SI lists possible isomers for a given molecular formula, based on prior studies. The selected literature for the general EF comparison (Fig. 2) is listed in SI Table S4 along

with relevant parameters and includes laboratory biomass burning studies (Koss et al., 2018); aircraft measurements of wildfire emissions (Hayden et al., 2022; Simpson et al., 2011; Permar et al., 2021); and compilations/databases (Akagi et al., 2011; 110 Andreae, 2019; Urbanski, 2014; Binte Shahid et al., 2024). Hayden et al. (2022) reported average EF for a comprehensive suite of VOCs and other trace gases from a mature boreal forest fire in Saskatchewan, Canada that had been burning for nearly two days (plume age  $\sim 14$  h, MCE = 0.82). Simpson et al. (2011) reported average EF for several gas-phase compounds and 57 VOCs from five Canadian boreal forest fire plumes, measured during the summer 2008 ARCTAS field mission (average MCE of 0.89). The Hayden et al. (2022) and Simpson et al. (2011) studies are the only two aircraft campaigns that have measured 115 comprehensive VOC emissions from Canadian boreal wildfires. Although not specific to Canadian boreal fires, EF for 161 VOCs from the recent WE-CAN aircraft study (Permar et al., 2021), are also used for literature comparison. Permar et al. (2021) sampled near-fire smoke plumes from twenty-four individual fires across the Western United States (average MCE of 0.90), with mixed coniferous ecosystems primarily dominated by pine, fir, and spruce trees, with the nearest transects with physical ages  $< 130$  min. The FIREX 2016 laboratory study (Koss et al., 2018; Selimovic et al., 2018) is also included given 120 the large range of fuels studied (predominantly biomass from the Western United States, but also including two Indonesian peat samples) and extensive characterization of VOC and trace gas emissions. The average EF across all studied biomass types from Koss et al. (2018) is used for general literature comparison (Section 3.2).

Several studies have compiled EF datasets for ‘Boreal Forest’ and ‘Peat’ fires that are based on laboratory and field studies. These datasets are used in wildfire emissions and smoke forecast models, including CFFEPS (Chen et al., 2019), GFAS (Kaiser 125 et al., 2012; Copernicus Atmosphere Monitoring Service, 2022), FINN (Wiedinmyer et al., 2023), GFED (Randerson et al., 2013), and BlueSky (AirFire Research Team, 2025). Among them, Binte Shahid et al. (2024) is a next-generation update of the original Akagi et al. (2011) emissions inventory, and Andreae et al. (2019) compilation is an update of the earlier Andreae & Merlot (2001) emissions inventory. For these datasets, the “Peat” fires assume a tropical forest overstory. Urbanski (2014) provides compiled EF separately for “Wildfire Boreal Forest” and “Boreal Forest Duff/Organic Soil”.

130 Fig. 5 in the manuscript and Fig. S5 display average VOC EF ( $\text{g kg}^{-1}$ ) as a function of fire-integrated MCE from this study and from the literature. The literature referenced is listed in Tables S4 and Table S5 with notes regarding the type of study, biomass, source table, average MCE, and additional notes. The additional literature in Table S5 expands on Table S4 to include EFs for specific fuels with a focus on peat fuels, organic soils, Ponderosa pine, and other coniferous fuels. In particular, Bertschi et al. (2003) and Yokelson et al. (2013) are referenced based on their relevance to the Urbanski (2014) profiles. Also included 135 are mean EF for PN, PN canopy, PN litter, and Indonesian peat from the FIREX 2016 laboratory study (Koss et al., 2018; Selimovic et al., 2018) and for black spruce (AK), PN, and Canadian peat (2 stack burns only) from the FLAME-4 laboratory campaign (Stockwell et al., 2015). It is worth noting that Urbanski et al. (2022) conducted controlled laboratory studies to determine EF for trace gases from surface fuels from the western U.S. and Canada (which included black spruce and jack pine needles and dead branches). However, only a limited number of VOCs were quantified in that study, and so it was not included 140 in the literature comparison. The Akagi et al. (2011) and Shahid et al. (2024) compilations do not report MCE for their “Boreal Forest” and “Peat” profiles, and so the MCE for “Wildfire Boreal Forest” (0.92) and “Boreal Forest Duff/Organic Soil” (0.79) from Urbanski (2014) were used.

The literature values in Fig. 5 and Fig. S5 are grouped into aircraft wildfire studies (orange triangles), laboratory studies (purple circles), and EF databases/compilations (open green triangles). The Urbanski (2014) EFs are shown as solid green triangles for their relevance to FireWork-CFFEPS (Chen et al., 2019). For clarity, the fuel type identities for this study are not distinguished, but the reader can ascertain the fuel identities with the knowledge that the average MCE for low moisture content fuels increases in the order PM (0.76), PF (0.77), SM (0.91), PN (0.93), and GR=MU (0.94). The wet PM and PF fuels have an MCE = 0.92, and MU (wet) has an MCE = 0.94. The 23 VOC compounds (plus CH<sub>4</sub>) chosen for display in Fig. 5 and Fig. S5 include key compounds across a range of compound classes. In addition to highlighting the relationship between EF and MCE for the VOC and fuel types in this study, these figures also provide insight regarding the consensus amongst literature studies.

### Section S6: Dependence of NMOC, $\sum$ VOCs, and individual VOC emission factors (EF) on modified combustion efficiency (MCE)

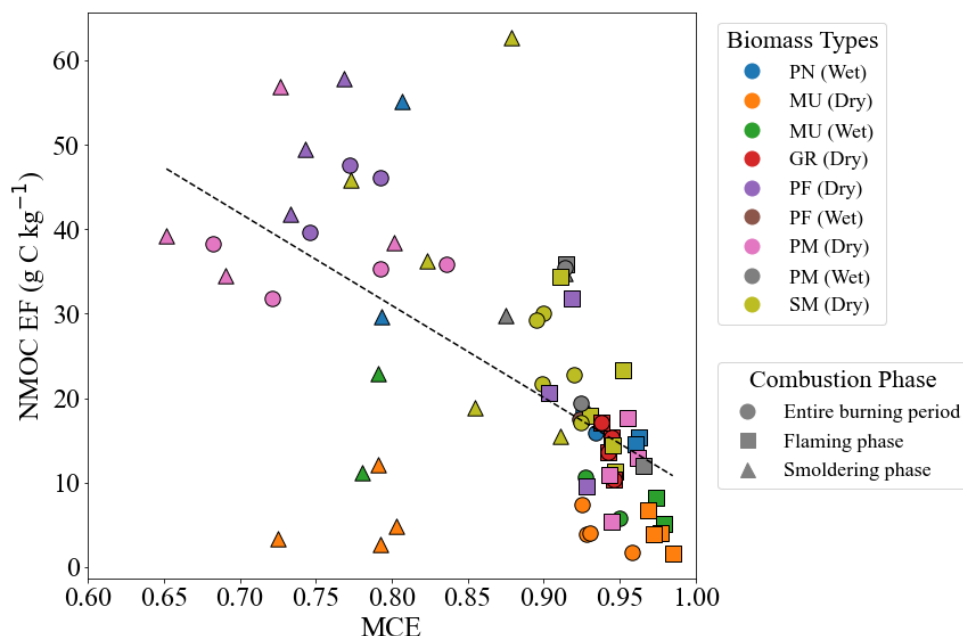


**Figure S3.** Relationship between individual burn NMOC EF ( $\text{g C kg}^{-1}$ ) and MCE for different biomass types and combustion phases. Symbols denote combustion phases (circle: entire burn, square: flaming, triangle: smoldering), while colors represent biomass types; this plot shows all individual burn data points. The dashed line indicates the least-squares linear fit to all data points, with slope (- 109), intercept (118), and  $R^2$  (0.38).

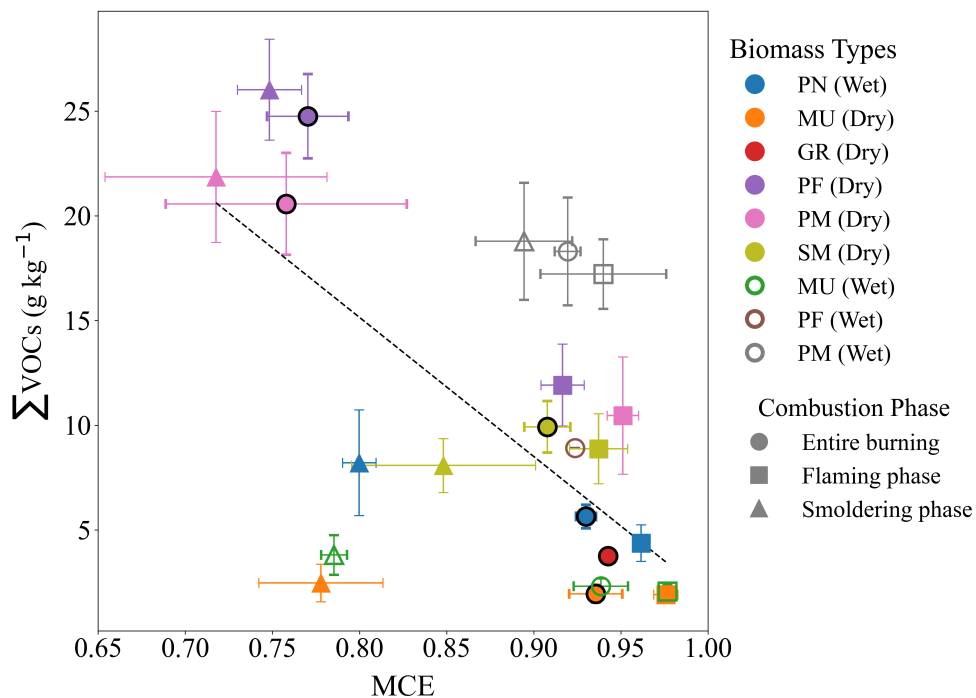


**Figure S4.**  $\sum \text{VOCs}$  ( $\text{g kg}^{-1}$ ) as a function of MCE across various biomass fuel types. Data are shown for the entire burning period (circles), flaming phase (squares), and smoldering phase (triangles). Vertical and horizontal error bars represent the standard deviation of the mean  $\sum \text{VOCs}$  and MCE, respectively. The dashed line indicates the linear regression fitted to the low-moisture content fuels (solid symbols), with slope (- 66), intercept (68), and  $R^2$  (0.53). The entire burn data are highlighted with a bold black outline, while open symbols denote MU (wet), PM (wet), and PF (wet) fuels.

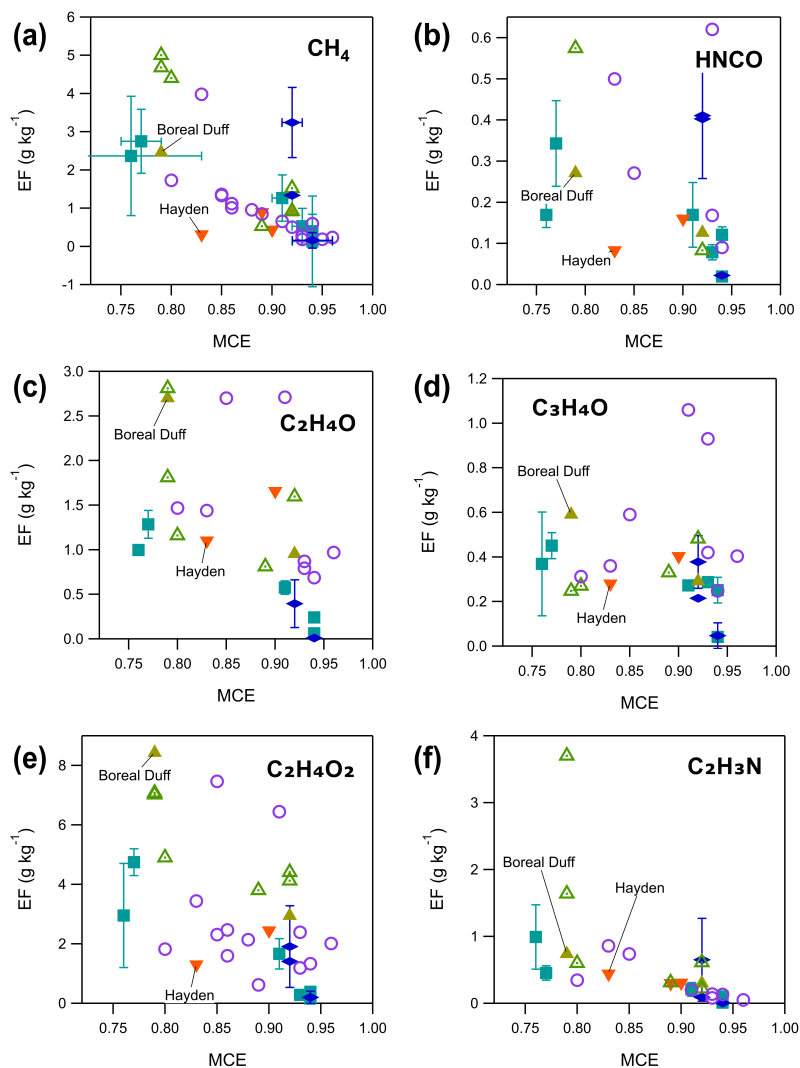


**Figure S5.** Mean VOC EF as a function of average fire-integrated MCE for low moisture content fuels (teal squares: PM, PF, SM, PN, GR, MU) and wet fuels (dark blue diamonds: PM, PF, MU). Error bars represent the standard deviation of the mean. Also shown are EFs from wildfire studies (orange triangles), (Hayden et al., 2022; Permar et al., 2021; Simpson et al., 2011), laboratory studies (purple circles) (Koss et al., 2018; Selimovic et al., 2018; Stockwell et al., 2015; Yokelson et al., 2013; Bertschi et al., 2003), and EF databases/compilations (open green triangles) (Akagi et al., 2011; Andreae, 2019; Binte Shahid et al., 2024), including Urbanski (2014) (Urbanski, 2014) “Boreal Forest Duff” and “Wildfire Boreal Forest” (solid green triangles) where available. The Hayden et al. (2022) aircraft study and the Urbanski (2014) “Boreal Duff” are tagged for additional clarity.

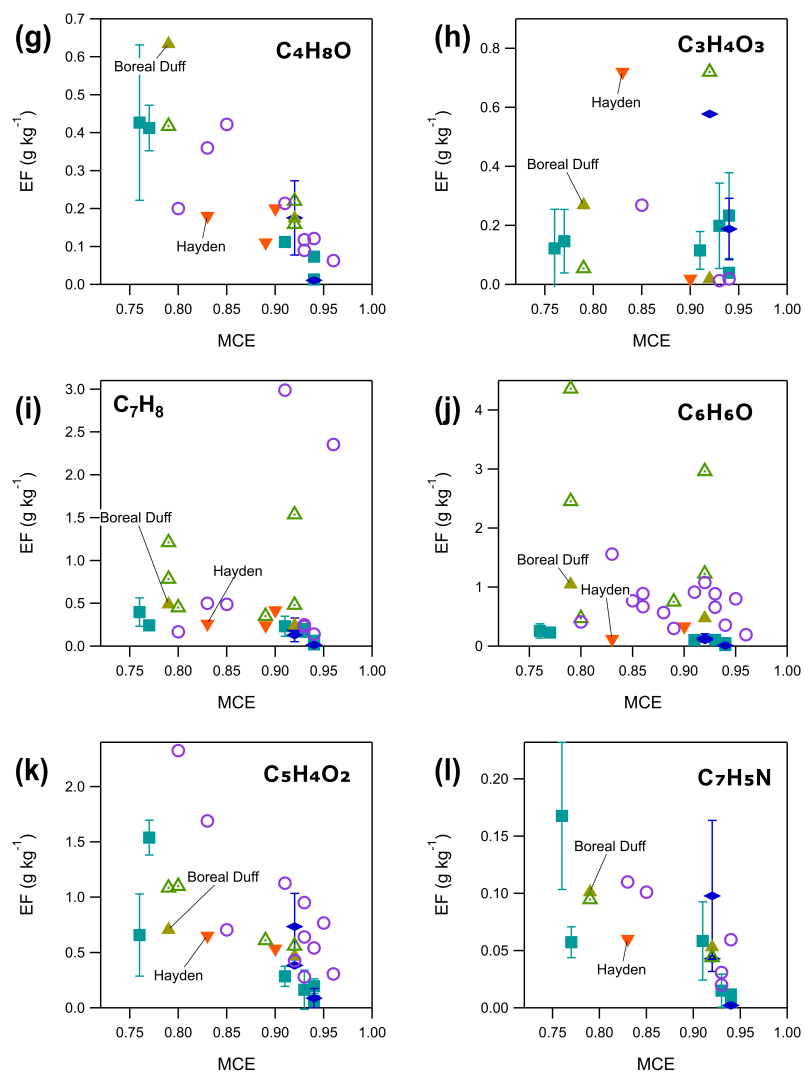


**Figure S5.** (continued)

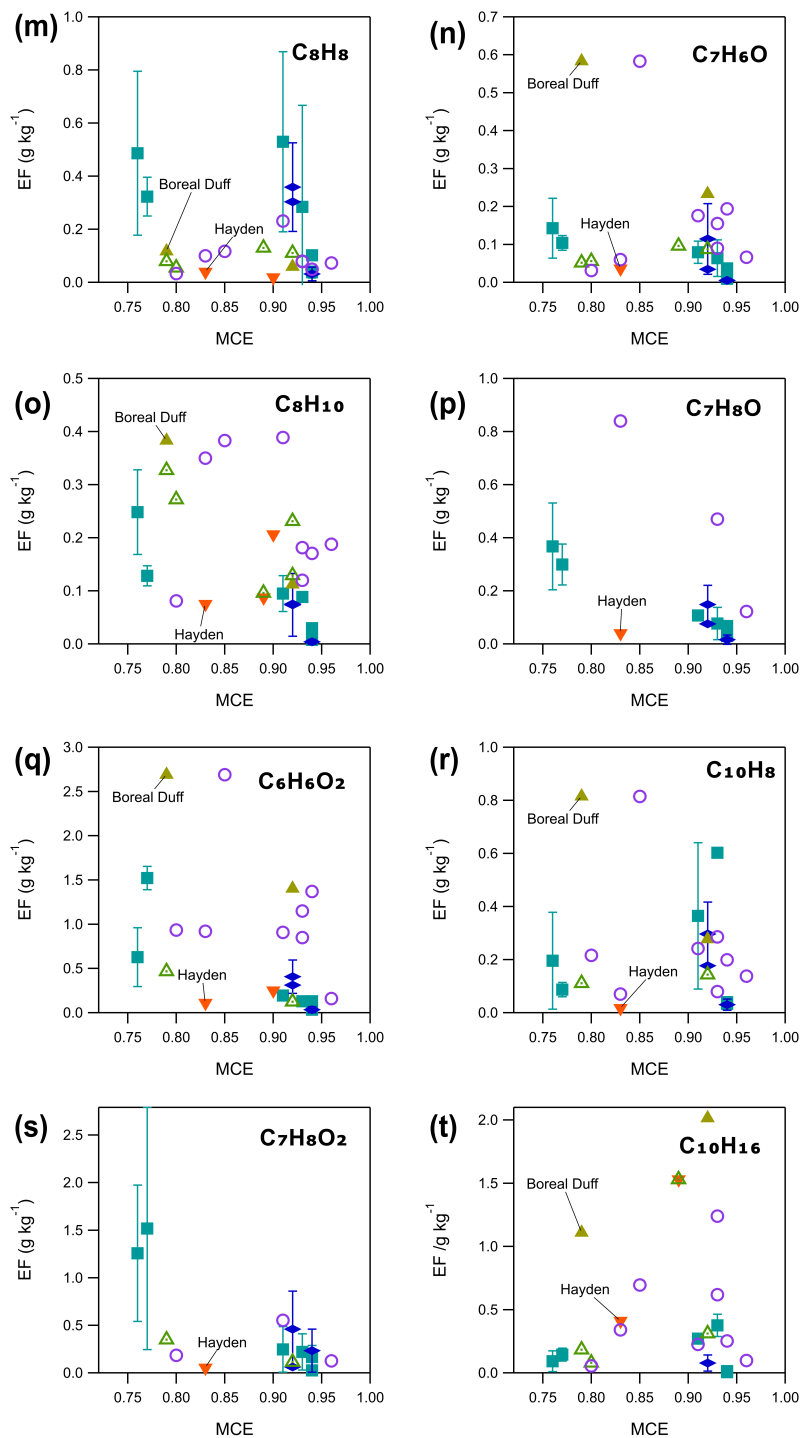


Figure S5. (continued)



## Section S7: Principal Component Analysis (PCA)

PCA is a multivariate statistical approach used to simplify complex datasets and to explore similarities, differences, and overall patterns among samples (Jolliffe and Cadima, 2016; Abdi and Williams, 2010; Bro and Smilde, 2014). PCA was performed using Python for data analysis and visualization. In this study, PCA was applied to the mean EF of the measured gaseous compounds during the entire burn phase for all biomass fuels. The input matrix consisted of biomass samples and EFs. Because EFs can vary in magnitude across compounds, the data were standardized by mean-centering and scaling each variable to unit variance (mean = 0 and standard deviation = 1). This standardization ensures that all compounds contribute equally to the analysis and prevents variables with large numerical values from dominating the results (Abdi and Williams, 2010). The PCA transforms the standardized variables into principal components ranked according to the amount of variance they explain, where the first principal component (PC1) captures the largest fraction of variability in the dataset, followed by PC2, which explains the next largest independent source of variance (Jolliffe and Cadima, 2016; Abdi and Williams, 2010).

The PCA scores plot provides a visual representation of similarities and differences among biomass samples, where the origin (0,0) represents the multivariate mean of the standardized dataset. Samples located near the origin exhibit VOC emission profiles closer to the overall average, whereas increasing distance from the origin indicates greater deviation from the mean emission pattern. Similarly, samples positioned closer together reflect more similar VOC emission characteristics, while greater separation between points indicates increased dissimilarity among biomass types (Jolliffe and Cadima, 2016; Abdi and Williams, 2010).

In this study, to explore drivers of emission variability between fuel types, PCA was performed using the mean EF data of each fuel measured during the entire burning (Fig. S6). Each point in Fig. S6 represents a specific fuel (under wet or dry conditions), defined by its EF profile across all 46 quantified VOCs as well as HONO. For the analysis of the entire burn, the first two principal components explain 73.1 % of the total variance, with PCA1 and PCA2 accounting for 54.6 % and 18.5 %, respectively.

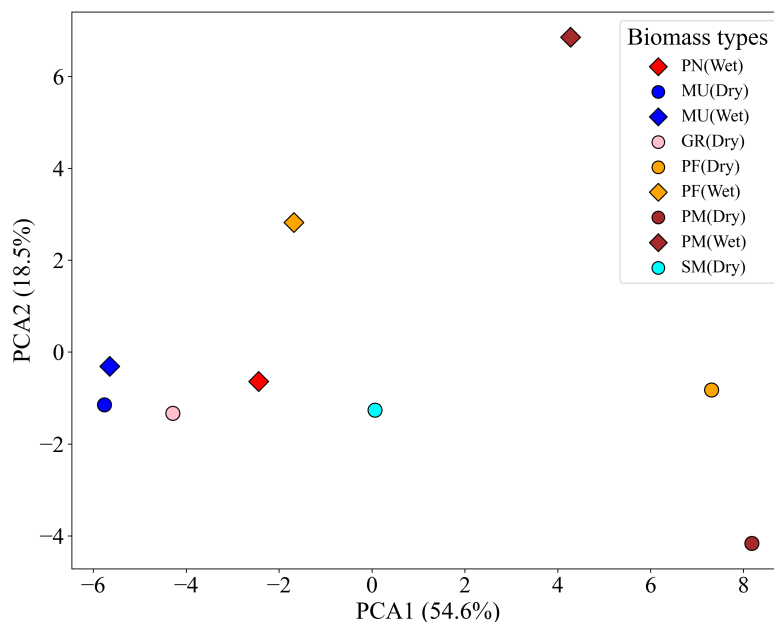


**Figure S6.** PCA performed using overall EF of species quantified in this study (46 VOC + HONO). PCA1 and PCA2 explain 56.4 % and 17.8 % of the total variance, respectively. Wet fuels are shown as diamonds and dry fuels as circles, with the six biomass types (PN, MU, GR, PF, PM, SM) as different colours.

175 MU (dry and wet) and GR (dry) fuels, all of which exhibit high combustion efficiency (mean MCE  $\sim 0.94$ ), cluster closely in the lower left quadrant, suggesting shared dominant compounds and combustion behavior, particularly for the two MU samples. On the other hand, the dry, peat-associated fuels, PF (dry) and PM (dry), burn with low MCE, characteristic of smoldering combustion (mean of 0.77 and 0.76, respectively), and are clearly separated to the right along PCA1. SM (dry) and PN (wet) burn with intermediate MCE (mean of 0.91 and 0.93, respectively) and are separated accordingly. Therefore, separation along PCA1 is largely explained by the characteristic MCE of the different biomass types, and the PCA analysis confirms the significant role of MCE on VOC emissions. Separation along PCA2 may be related to fuel moisture content. Although MU (wet) and PN (wet) samples are labelled as ‘wet’ since they were undried, their mean moisture contents were relatively low (8 % and 13 %, respectively) and comparable to those of the dried samples, including MU (4 %), GR (20 %), SM (14 %), PF (8 %), and PM (15 %). These low-moisture content fuels all cluster along PCA2, with the exception of PM (dry), which shows some separation to the lower quadrant. In contrast, the raw (undried) peat-associated fuels (PF and PM) were indeed ‘wet’ with very high moisture contents (51 and 100 %, respectively). Accordingly, the wet peat-associated fuels are shifted upward along PCA2, indicating moisture-driven changes in their VOC emission profiles. Noted that, these samples were so wet that the fire was extinguished soon after the flaming stage, leaving a significant unburnt sample, which also explains the higher MCE (0.92 for both PM (wet) and PF (wet) and shift for these fuels along PCA1 to the left. To a certain extent, the comparison of wet peat fuels to dry peat fuels reflects a flaming vs. full-burn (dominated by smoldering) comparison.

180

185

190

Correlation plots of the mean overall VOC EF for select fuel pairs are presented (SI Fig. S7) and further illustrate that VOC emission profiles vary across fuel types and moisture conditions. The correlation plots of the mean EF for quantified VOCs for selected fuel pairs presented in SI Fig. S3 corroborate the results of the PCA analysis, as fuel pairs that are poorly correlated (low  $R^2$ ) generally show greater separation on the scores plot. An exception is GR (dry) and MU (dry), which are poorly correlated ( $R^2 = 0.31$ ) despite both burning with high MCE and clustering on the PCA scores plot. The correlation between MU (dry) vs. MU (wet) is good ( $R^2 = 0.94$ ), indicating that moisture content exerts minimal influence on MU's emission profiles, which is consistent with the relatively small difference in their measured moisture contents.

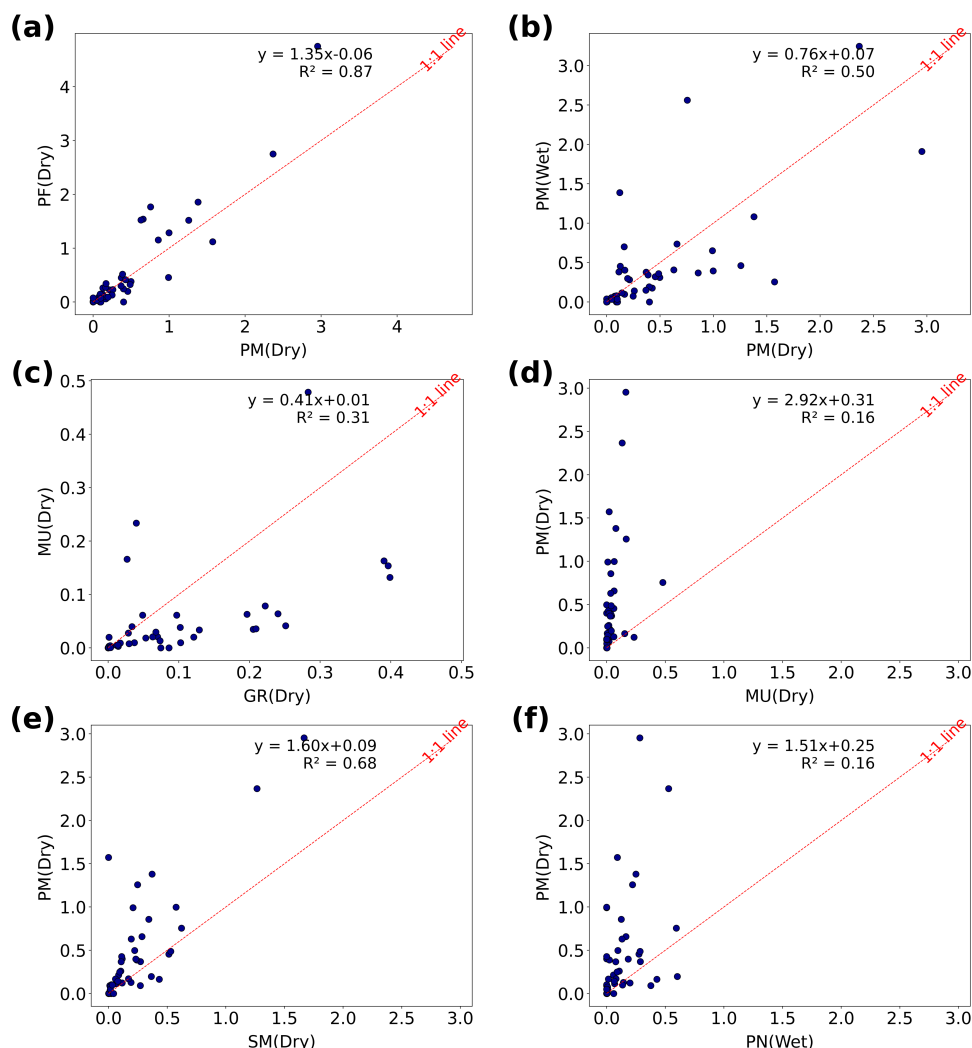


**Figure S7.** Correlation plots of mean, overall VOC EF (g kg<sup>-1</sup>) for select biomass fuel pairs. The red line indicates the 1:1 line.

## Section S8: Reactive nitrogen emission factors

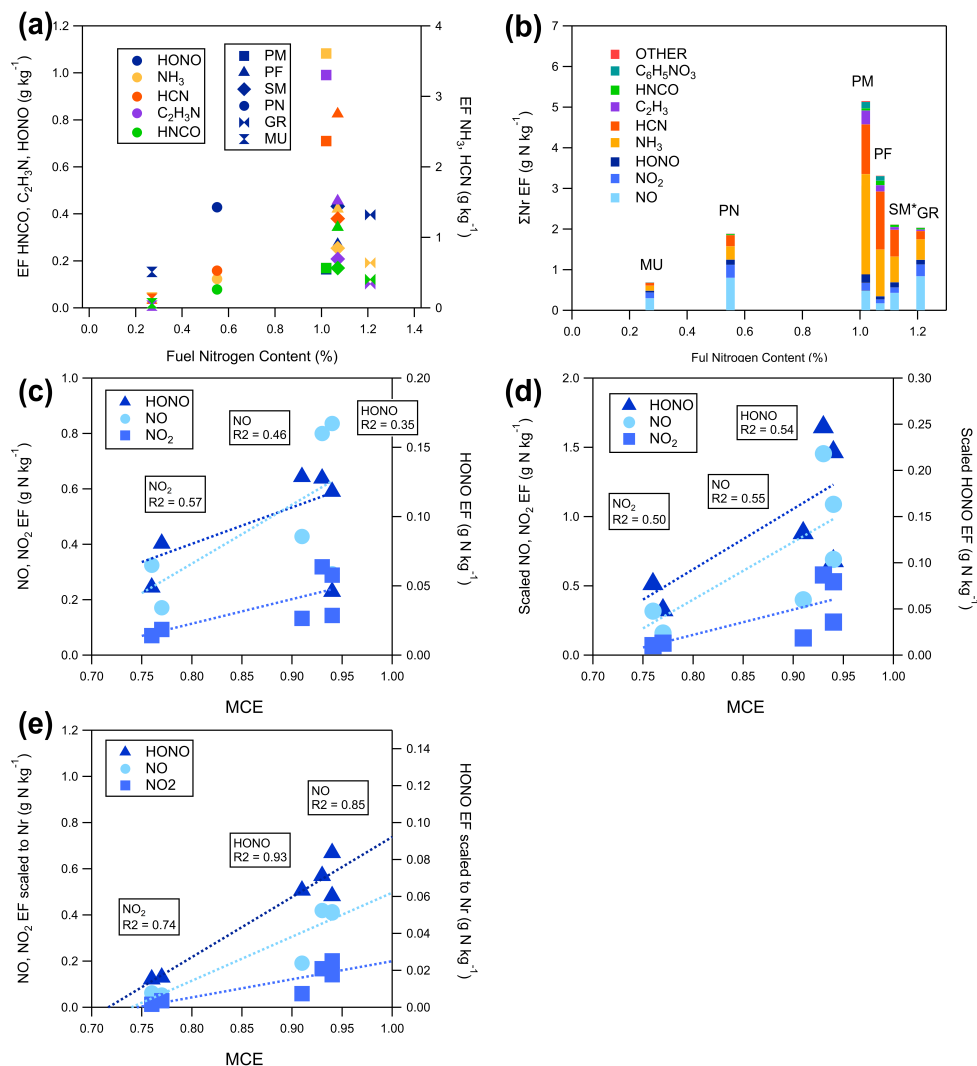


**Figure S8.** (a) Mean reactive nitrogen (Nr) EFs ( $\text{g N kg}^{-1}$ ) as a function of fuel nitrogen content (%); (b) mean total Nr ( $\Sigma\text{Nr}$ ) EF ( $\text{g N kg}^{-1}$ ) as a function of fuel nitrogen content (%); mean EF ( $\text{g N kg}^{-1}$ ) as a function of MCE for oxidized Nr species (NO,  $\text{NO}_2$ , HONO) in (c), with the same data but scaled to the fuel nitrogen content in (d) and scaled to  $\Sigma\text{Nr}$  in (e). Linear fits to the data are shown as dashed lines with  $R^2$  values displayed on the figures. OTHER = sum of  $\text{C}_2\text{H}_3\text{NO}$ ,  $\text{C}_3\text{H}_3\text{NO}_2$ ,  $\text{C}_2\text{H}_5\text{NO}_3$ ,  $\text{C}_7\text{H}_5\text{N}$ . Data shown for overall (entire burn), low-moisture content fuels only: PM (dry), PF (dry), SM (dry), PN (wet), MU (dry), GR (dry). \*The  $\Sigma\text{Nr}$  for SM is shifted in Fig. (b) for display purposes since its fuel nitrogen content overlaps with PF (both 1.07 %). Error bars showing the standard deviation of the mean are omitted for clarity of presentation.

Section S9: Additional Canadian Forest Fire Emissions Prediction System (CFFEPS) details

200 Allocation factors for combustion stages:

In CFFEPS (Chen et al., 2019), the amount of fuel consumed is calculated as the product of the burn area and the total fuel consumption (TFC, kg of dry biomass m<sup>-2</sup>), which is the sum of crown fuel consumption (CFC) and surface fuel consumption (SFC). CFFEPS divides combustion into flaming, smoldering, and residual stages based on fixed allocation factors: for CFC, canopy allocation factors are 94 % flaming combustion and 6 % smoldering combustion. For SFC, the allocation factors are  
205 split into three ground layers: litter (top 1.2 cm, 90 % flaming, 10 % smoldering), upper duff (1.2–7 cm depth, 10 % flaming, 70 % smoldering, 20 % residual), and lower duff (> 7 cm depth, 20 % smoldering, 80 % residual). GR is considered a surface-only fuel and is allocated separately, at 95 % flaming and 5 % smoldering. The burn depth is calculated from the SFC and fuel density, according to 14 Fire Behavior Prediction (FBP) fuel types.

Section S10: Dependence of NMOC<sub>G</sub> (g kg<sup>-1</sup>) on MCE

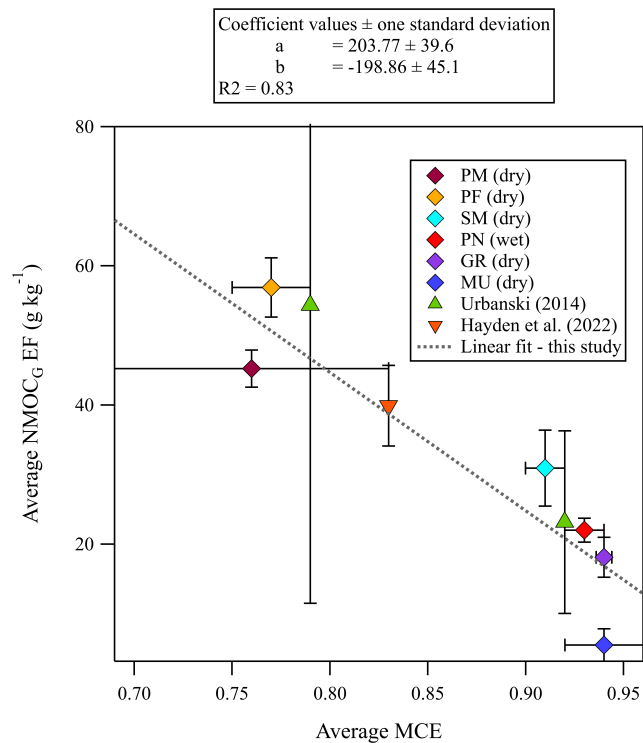


**Figure S9.** Average NMOC<sub>G</sub> EF (g kg<sup>-1</sup>) as a function of average MCE for low-moisture content fuels from this study (diamonds). The dashed grey line is a linear fit to the study data. The average NMOC<sub>G</sub> EF from Hayden et al. (2022) (orange inverted triangle) and Urbanski (2014), “Boreal forest duff” and “Wildfire boreal forest” (green triangles), are also plotted.

- Abdi, H. and Williams, L. J.: Principal component analysis, Wiley Interdiscip. Rev. Comput. Stat., 2, 433–459, <https://doi-org/10.1002/wics.101>DigitalObjectIdentifier(DOI), 2010.
- AirFire Research Team: BlueSky Modeling Framework. <https://www.airfire.org/data/bluesky> (last access: 17 December 2025), 2025.
- Akagi, S., Yokelson, R. J., Wiedinmyer, C., Alvarado, M. J., Reid, J. S., Karl, T., Crounse, J. D., and Wennberg, P. O.: Emission factors  
 215 for open and domestic biomass burning for use in atmospheric models, Atmos. Chem. Phys., 11, 4039–4072, <https://doi.org/10.5194/acp-11-4039-2011>, 2011.
- Andreae, M. O.: Emission of trace gases and aerosols from biomass burning—an updated assessment, Atmos. Chem. Phys., 19, 8523–8546, <https://doi.org/10.5194/acp-19-8523-2019>, 2019.
- Bertschi, I., Yokelson, R. J., Ward, D. E., Babbitt, R. E., Susott, R. A., Goode, J. G., and Hao, W. M.: Trace gas and particle emissions from  
 220 fires in large diameter and belowground biomass fuels, J. Geophys. Res. Atmos., 108, <https://doi.org/10.1029/2002JD002100>, 2003.
- Binte Shahid, S., Lacey, F. G., Wiedinmyer, C., Yokelson, R. J., and Barsanti, K. C.: NEIVAv1. 0: Next-generation Emissions InVentory expansion of Akagi et al.(2011) version 1.0, Geosci. Model Dev., 17, 7679–7711, <https://doi.org/10.5194/gmd-17-7679-2024>, 2024.
- Bro, R. and Smilde, A. K.: Principal component analysis, Anal. Methods, 6, 2812–2831, <https://doi.org/10.1039/C3AY41907J>, 2014.
- Chen, J., Anderson, K., Pavlovic, R., Moran, M. D., Englefield, P., Thompson, D. K., Munoz-Alpizar, R., and Landry, H.: The FireWork v2.  
 225 0 air quality forecast system with biomass burning emissions from the Canadian Forest Fire Emissions Prediction System v2. 03, Geosci. Model Dev., 12, 3283–3310, <https://doi.org/10.5194/gmd-12-3283-2019>, 2019.
- Coggon, M. M., Stockwell, C. E., Claflin, M. S., Pfannerstill, E. Y., Xu, L., Gilman, J. B., Marcantonio, J., Cao, C., Bates, K., Gkatzelis, G. I., et al.: Identifying and correcting interferences to PTR-ToF-MS measurements of isoprene and other urban volatile organic compounds, Atmos. Meas. Tech., 17, 801–825, <https://doi.org/10.5194/amt-17-801-2024>, 2024.
- 230 Copernicus Atmosphere Monitoring Service: Global fire emissions (CAMS GFAS). <https://atmosphere.copernicus.eu/global-fire-emissions> (last access: 23 December 2025), 2022.
- Gilman, J., Lerner, B., Kuster, W., Goldan, P., Warneke, C., Veres, P., Roberts, J., De Gouw, J., Burling, I., and Yokelson, R.: Biomass burning emissions and potential air quality impacts of volatile organic compounds and other trace gases from fuels common in the US, Atmos. Chem. Phys., 15, 13 915–13 938, <https://doi.org/10.5194/acp-15-13915-2015>, 2015.
- 235 Hayden, K. L., Li, S.-M., Liggio, J., Wheeler, M. J., Wentzell, J. J., Leithead, A., Brickell, P., Mittermeier, R. L., Oldham, Z., Mihele, C. M., et al.: Reconciling the total carbon budget for boreal forest wildfire emissions using airborne observations, Atmos. Chem. Phys., 22, 12 493–12 523, <https://doi.org/10.5194/acp-22-12493-2022>, 2022.
- Jensen, A. R., Koss, A. R., Hales, R. B., and de Gouw, J. A.: Measurements of volatile organic compounds in ambient air by gas-chromatography and real-time Vocus PTR-TOF-MS: calibrations, instrument background corrections, and introducing a PTR Data Toolkit,  
 240 Atmos. Meas. Tech., 16, 5261–5285, <https://doi.org/10.5194/amt-16-5261-2023>, 2023.
- Jolliffe, I. T. and Cadima, J.: Principal component analysis: a review and recent developments, Philos. Trans. Roy. Soc. A, 374, 20150 202, <https://doi-org/10.1098/rsta.2015.0202>, 2016.
- Kaiser, J., Heil, A., Andreae, M., Benedetti, A., Chubarova, N., Jones, L., Morcrette, J.-J., Razinger, M., Schultz, M., Suttie, M., et al.: Biomass burning emissions estimated with a global fire assimilation system based on observed fire radiative power, Biogeosciences, 9, 527–554, <https://doi.org/10.5194/bg-9-527-2012>, 2012.
- 245

- Koch, B. P. and Dittmar, T.: From mass to structure: An aromaticity index for high-resolution mass data of natural organic matter, *Rapid Commun. Mass Spectrom.*, 20, 926–932, <https://doi-org/10.1002/rcm.2386>, 2006.
- Koss, A. R., Sekimoto, K., Gilman, J. B., Selimovic, V., Coggon, M. M., Zarzana, K. J., Yuan, B., Lerner, B. M., Brown, S. S., Jimenez, J. L., et al.: Non-methane organic gas emissions from biomass burning: identification, quantification, and emission factors from PTR-ToF during the FIREX 2016 laboratory experiment, *Atmos. Chem. Phys.*, 18, 3299–3319, <https://doi.org/10.5194/acp-18-3299-2018>, 2018.
- Link, M. F., Claflin, M. S., Cecelski, C. E., Akande, A. A., Kilgour, D., Heine, P. A., Coggon, M., Stockwell, C. E., Jensen, A., Yu, J., et al.: Product ion distributions using  $\text{H}_3\text{O}^+$  proton-transfer-reaction time-of-flight mass spectrometry (PTR-ToF-MS): mechanisms, transmission effects, and instrument-to-instrument variability, *Atmospheric Measurement Techniques*, 18, 1013–1038, <https://doi.org/10.5194/amt-18-1013-2025>, 2025.
- Moraes, A. H., Talebian, S., Afroz, R., Al-Jabiri, M. H., Chan, A. W. H., Chang, R. Y.-W., Chen, K., Corbin, J. C., Drinovec, L., Isenor, B. H., Lee, A., Liggio, J., Liu-Kang, C., Marshall, G., Moallemi, A., Mocnik, G., Moussa, S. G., Olfert, O., Saleh, M., Sipkens, T. A., Shen, H., Wentzell, J. J. B., Wren, S. N., Yus-Díez, J., Hayes, P. L., Abbatt, J. P. D., Olfert, J., and Zhao, R.: Combustion Characteristics and Emission Factors of Trace Gases and Particulate Matter from Biomass Relevant to Canadian Wildfires: Overview of the 2024 BBCan Campaign, *ESS Open Archive [preprint]*, <https://doi.org/10.22541/essoar.15002871/v1>, 7 May 2026.
- Pagonis, D., Sekimoto, K., and De Gouw, J.: A library of proton-transfer reactions of  $\text{H}_3\text{O}^+$  ions used for trace gas detection, *J. Am. Soc. Mass Spectrom.*, 30, 1330–1335, <https://doi-org/10.1007/s13361-019-02209-3>, 2019.
- Permar, W., Wang, Q., Selimovic, V., Wielgasz, C., Yokelson, R. J., Hornbrook, R. S., Hills, A. J., Apel, E. C., Ku, I.-T., Zhou, Y., et al.: Emissions of trace organic gases from Western US wildfires based on WE-CAN aircraft measurements, *J. Geophys. Res. Atmos.*, 126, e2020JD033 838, <https://doi.org/10.1029/2020JD033838>, 2021.
- Pfannerstill, E. Y., Arata, C., Zhu, Q., Schulze, B. C., Woods, R., Harkins, C., Schwantes, R. H., McDonald, B. C., Seinfeld, J. H., Bucholtz, A., et al.: Comparison between spatially resolved airborne flux measurements and emission inventories of volatile organic compounds in Los Angeles, *Environmental Science & Technology*, 57, 15 533–15 545, <https://doi.org/10.1021/acs.est.3c03162>, 2023.
- Randerson, J., van der Werf, G., Giglio, L., Collatz, G., and Kasibhatla, P.: Global fire emissions database, version 3.1, ORNL DAAC, <https://doi.org/10.3334/ORNLDAAC/1191>, 2013.
- Roson, M. L., Schmidt, S. A., Choudhary, V., Johnson, T. A., de la Mata, A. P., Harynuk, J. J., and Zhao, R.: Comprehensive analysis of emissions from wood and cow dung burning using chemometrics and two-dimensional gas chromatography, *Chemosphere*, 366, 143 445, <https://doi-org/10.1016/j.chemosphere.2024.143445>, 2024.
- Sekimoto, K., Li, S.-M., Yuan, B., Koss, A., Coggon, M., Warneke, C., and De Gouw, J.: Calculation of the sensitivity of proton-transfer-reaction mass spectrometry (PTR-MS) for organic trace gases using molecular properties, *Int. J. Mass Spectrom.*, 421, 71–94, <https://doi-org/10.1016/j.ijms.2017.04.006>, 2017.
- Selimovic, V., Yokelson, R. J., Warneke, C., Roberts, J. M., De Gouw, J., Reardon, J., and Griffith, D. W.: Aerosol optical properties and trace gas emissions by PAX and OP-FTIR for laboratory-simulated western US wildfires during FIREX, *Atmos. Chem. Phys.*, 18, 2929–2948, <https://doi.org/10.5194/acp-19-3905-2019>, 2018.
- Simpson, I. J., Akagi, S., Barletta, B., Blake, N., Choi, Y., Diskin, G., Fried, A., Fuelberg, H., Meinardi, S., Rowland, F., et al.: Boreal forest fire emissions in fresh Canadian smoke plumes: C 1-C 10 volatile organic compounds (VOCs),  $\text{CO}_2$ , CO,  $\text{NO}_2$ , NO, HCN and  $\text{CH}_3\text{CN}$ , *Atmos. Chem. Phys.*, 11, 6445–6463, <https://doi.org/10.5194/acp-11-6445-2011>, 2011.

- Stockwell, C., Veres, P., Williams, J., and Yokelson, R.: Characterization of biomass burning emissions from cooking fires, peat, crop residue, and other fuels with high-resolution proton-transfer-reaction time-of-flight mass spectrometry, *Atmos. Chem. Phys.*, 15, 845–865, <https://doi.org/10.5194/acp-15-845-2015>, 2015.
- 285 Urbanski, S.: Wildland fire emissions, carbon, and climate: Emission factors, *For. Ecol. Manage.*, 317, 51–60, <https://doi.org/10.1016/j.foreco.2013.05.045>, 2014.
- Wiedinmyer, C., Kimura, Y., McDonald-Buller, E. C., Emmons, L. K., Buchholz, R. R., Tang, W., Seto, K., Joseph, M. B., Barsanti, K. C., Carlton, A. G., et al.: The Fire Inventory from NCAR version 2.5: an updated global fire emissions model for climate and chemistry applications, *Geosci. Model Dev.*, 16, 3873–3891, <https://doi.org/10.5194/gmd-16-3873-2023>, 2023.
- 290 Yokelson, R. J., Burling, I., Gilman, J., Warneke, C., Stockwell, C., De Gouw, J., Akagi, S., Urbanski, S., Veres, P., Roberts, J., et al.: Coupling field and laboratory measurements to estimate the emission factors of identified and unidentified trace gases for prescribed fires, *Atmos. Chem. Phys.*, 13, 89–116, <https://doi.org/10.5194/acp-13-89-2013>, 2013.